# Electronic Supplementary Information

# Direct synthesis of Co@Al-MCM-41 catalyst from conventional $Co/SiO_2$ catalyst

Jiang-Yong Liu, [a] Jian-Feng Chen *[a] and Yi Zhang *[a]

State Key Laboratory of Organic-Inorganic Composites; Research Centre of the Ministry of Education for High Gravity Engineering and Technology; Beijing University of Chemical Technology, Beijing 100029, China

*Corresponding author: chenjf@mail.buct.edu.cn; yizhang@mail.buct.edu.cn

Contents

**ESI-1**. Experimental details.

## Catalyst Preparation

The conventional precursor catalyst $Co/SiO_2$ was the same as that utilized in our previous study.[1]

For the preparation of the cobalt-imbedded Al-containing MCM-41 catalyst (denoted as Co@Al-MCM-41), Cetyltrimethylammonium bromide (CTAB) was employed as a template surfactant. For the crystallization of the mesoporous molecular sieve, the dissolved silica from the precursor $Co/SiO_2$ during the hydrothermal procedure was the only Si source and $Al(NO_3)_3 \cdot 9H_2O$ was selected as the Al source. The catalyst was synthesized from a mixture of reactants using the following molar composition: 1.0 $SiO_2$ ($Co/SiO_2$): 0.125 CTAB: 0.02 Al: 0.30 TMAOH (tetramethylammonium hydroxide): 8.0 $NH_3$: 50.0 $H_2O$. In a typical synthesis procedure, CTAB was firstly dissolved in the deionized water under continuous stirring at 313 K for 1.0 h, and then the required amount of TMAOH was added to the solution. After 30 min stirring of the mixture, $Al(NO_3)_3 \cdot 9H_2O$ was added and stirred for another 30 min. After that, the precursor $Co/SiO_2$ power was added and allowed for vigorous stirring for 6 h. Finally, after the addition of a given volume of $NH_3 \cdot H_2O$, the suspension was transferred into a Teflon-lined stainless-steel autoclave and heated at 393 K for 48 h. After crystallization, the sample was obtained by filtration and washed thoroughly with deionized water and ethanol. The solid product was dried at 373 K for 12 h, and then the organic template settled in the mesopores was removed by calcination in air at 823 K for 6 h.

For a comparison purpose, the supported Co/Al-MCM-41 with nominal 20 wt% cobalt loading was prepared as well. The catalyst support Al-MCM-41 was synthesized with the similar procedure of the above Co@Al-MCM-41 catalyst except that the Si source was changed to the pure $SiO_2$ used in the

$Co/SiO_2$ catalyst. The impregnation process was the same as that described in our previous study.[13]

## Catalyst Characterization

The small-angle X-ray diffraction patterns (SA-XRD) were obtained on a Rigaku D/max - 2500VB2+/PC diffractometer (40 kV, 50 mA) using Cu Kα radiation (λ = 0.154056 nm) within the 2θ range of 0.5-10°, while the WA-XRD measurements were scanned at 40 kV and 200 mA between the 2θ range of 5-90°. The $Co_3O_4$ particle size was evaluated by the Scherrer equation, and the metallic cobalt size of the reduced catalyst was measured by the equation: $d\ (Co^0) = 0.75 \cdot d\ (Co_3O_4)$.[2] The lattice parameter ($a_0$) for a hexagonal structure was obtained from the ($d_{100}$) spacing using the following equation:[3]

$$a_0 = \frac{2d_{100}}{\sqrt{3}}$$

$N_2$ isothermal adsorption-desorption measurement at 77 K was conducted with a Micromeritics ASAP 2010 system. Prior to the test, the samples were outgassed at 473 K for 5 h. The surface area of the samples was determined by the Brunauer–Emmett–Teller (BET) method, while the pore volume was calculated at a relative pressure ($P/P_0$) of about 0.99, where $P$ and $P_0$ are the measured and equilibrium pressures, respectively. The pore size distribution curves were obtained with the Barrett–Joyner–Halenda (BJH) method from the desorption branches of the isotherms.

The Transmission electron microscopy (TEM) images were obtained on a JEOL JEM-3010 microscope. The samples were dispersed with ethanol and then a drop of the suspension was deposited onto a holey carbon coated copper grid.

The high-angle annular dark-field scanning-transmission electron microscopy (HAADF-STEM) images were acquired using a Tecnai G2 F20 S-Twin high-resolution transmission electron microscope

with an energy-diffusive X-ray spectroscopy attachment. The preparation of the samples was similar with that of the TEM analysis.

The $^{27}$Al MAS-NMR spectra of the calcined samples were recorded on a 300 MHz solid-state Bruker AV300 spectrometer ($B_0$=7.05 T). The resonance frequency was 78.2 MHz and the spin rate of the samples was 8.0 kHz.

The X-ray fluorescence (XRF) analysis was conducted on a XRF-1800 spectrometer to obtain the elementary composition of the samples.

The reduction behavior of the catalysts was measured by the hydrogen temperature programmed reduction ($H_2$-TPR) experiments in a quartz-made microreactor. The temperature range was set between 323 K and 1173 K in a flow of 10% $H_2$/Ar (vol.) with a ramping rate of 10 K/min. The hydrogen consumption was recorded by analyzing the effluent gas with the thermal conductivity detector.

The XPS data were collected on a Thermo, Fisher Scientific ESCALAB 250 spectrometer in the constant analyzer energy (CAE) mode, with an Al Kα monochromatized X-ray source (1486.6 eV). The survey spectra were measured at 30 eV pass energy.

The $NH_3$-TPD experiment was performed on a flow reactor equipped with a thermal conductivity detector. Prior to the $NH_3$ adsorption, the samples were pretreated at 473 K for 1 h in a flow of He and then cooled down to 373 K. Subsequently, ammonia was introduced and maintained for 1 h. The physically adsorbed $NH_3$ was removed by purging with a He flow at 373 K until the baseline was flat. Finally, the desorption step was carried out in He with a heating rate of 10 K/min, up to 923 K.

## Catalyst Reaction

The FTS reaction was performed on a fixed-bed reactor. The reaction temperature was carefully

controlled by a thermocouple inserted into the catalyst bed. Before reaction, the catalyst loaded in the middle of the reactor was reduced in situ at atmospheric pressure in a $H_2$ gas flow at 673 K for 10 h. Afterwards, the syngas with a $H_2$/CO ratio of 2.0 was switched on and the pressure was slightly increased to 1.0 MPa. The reaction was carried out at 523 K and $W_{catalyst}/F_{syngas}$ was 5.0 $g \cdot h \cdot mol^{-1}$, using 0.5g catalyst. The feed gas contained 5 % argon, which was applied as an internal standard to calculate the carbon monoxide conversion. The reaction products were analyzed by gas chromatography. The apparatus, method and procedure have been described in detail elsewhere.[13]All the analysis results were summed up and calculated in terms of carbon mol percentage (c-mol %).

**ESI-2**. Fig. S1. Small-angle XRD patterns of the samples.

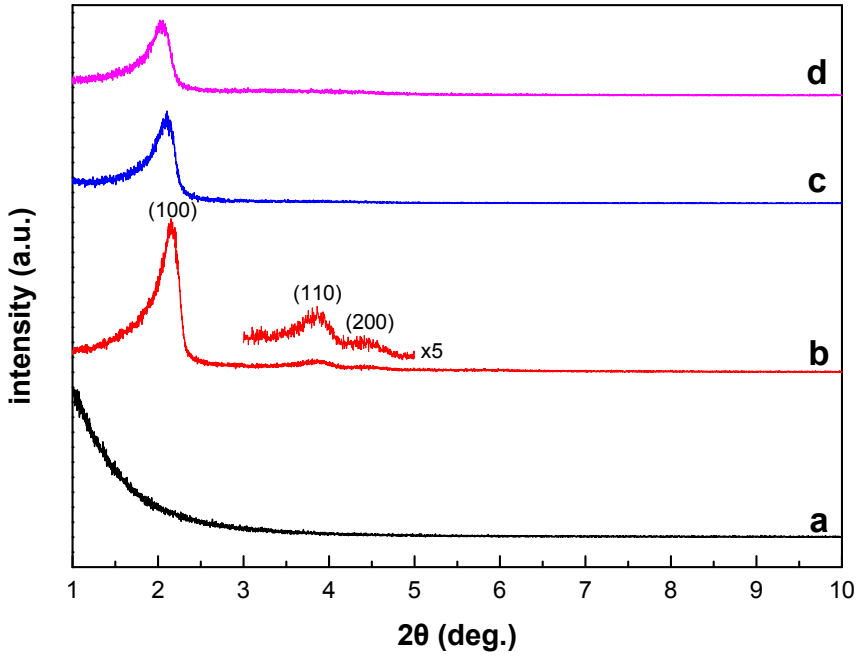


**Fig. S1.** Small-angle XRD patterns of the samples: (a) $SiO_2$, (b) Al-MCM-41, (c) Co/Al-MCM-41, (d) Co@Al-MCM-41.

**ESI-3**. Table S1 Textural and structural characteristics of the synthesized samples.

**Table S1.** Textural and structural characteristics of the synthesized samples.

| Samples | $d100$[a] (Å) | $a_0$[b] (Å) | $S_{BET}$[c] ($m^2/g$) | $V_p$[d] ($cm^3/g$) | $D_{BJH}$[e] (Å) |
|---|---|---|---|---|---|
| Al-MCM-41 | 40.3 | 46.5 | 958 | 0.95 | 29.3 |
| Co/Al-MCM-41 | 43.4 | 50.1 | 507 | 0.43 | 26.1 |
| Co@Al-MCM-41 | 42.0 | 48.5 | 689 | 0.66 | Bimodality [f] |

a Interplanar distance of basal reflection ($d_{100}$).

b Lattice parameter for a hexagonal structure ($a_0$).

c Surface area measured by the Brunauer–Emmett–Teller (BET) analysis method ($S_{BET}$).

d Pore volume obtained at relative pressure of 0.99 ($V_p$).

e Pore diameter determined from the desorption isotherms by the Barret–Joyner–Halenda (BJH) method ($D_{BJH}$).

f A bimodal pore size distribution (PSD) with a main peak at 30.9 Å and an additional peak at 38.4 Å .

**ESI-4.** Fig. S2 TEM images of the pure Al-MCM-41sample.

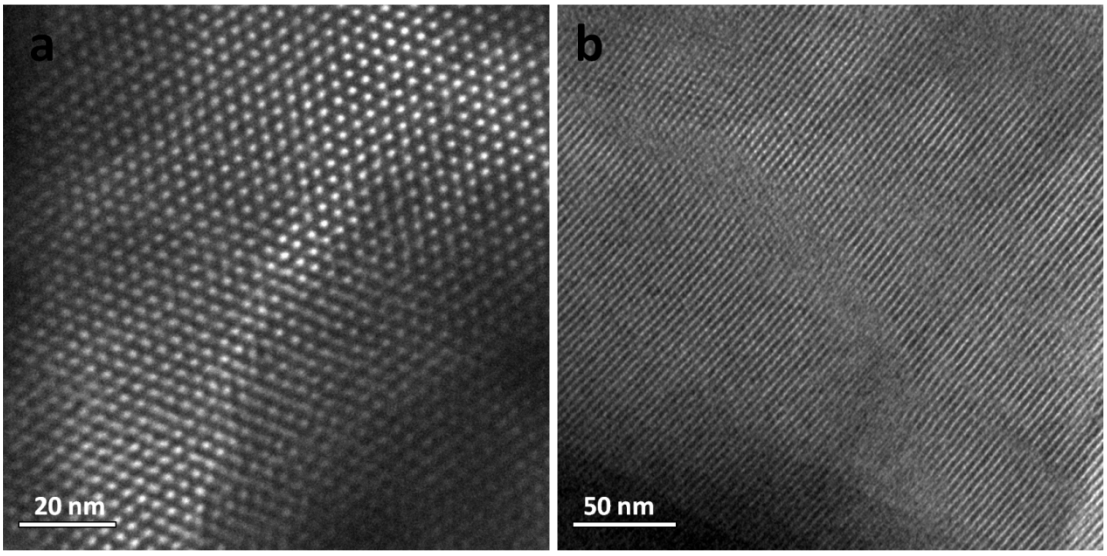


**Fig. S2.** TEM images of the pure Al-MCM-41 in the direction (a) parallel to the pore axis and (b) perpendicular to the pore axis.

**ESI-5.** Fig. S3 Nitrogen adsorption–desorption isotherms and the pore size distributions for the samples.

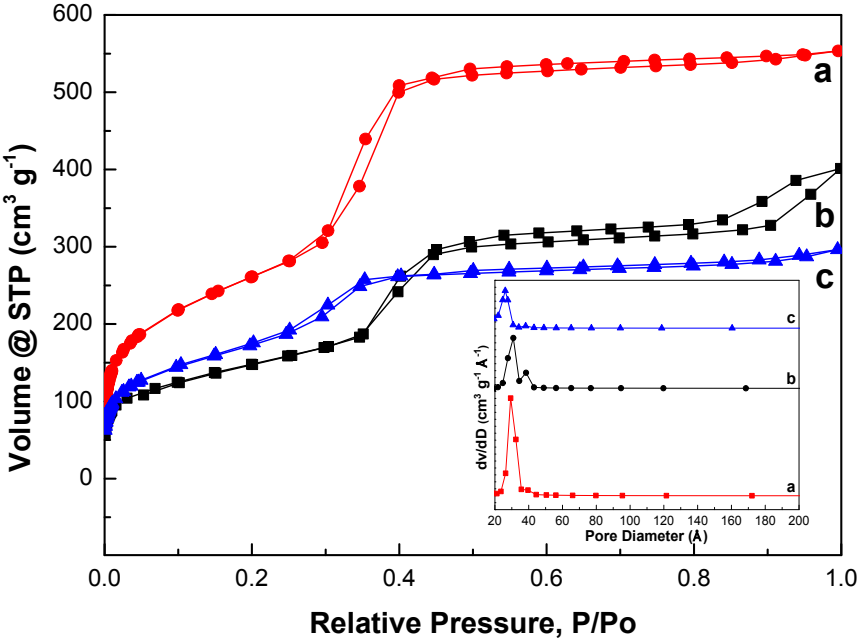


**Fig. S3.** Nitrogen adsorption–desorption isotherms and the pore size distributions (inset) for the samples: (a) Al-MCM-41, (b) Co@Al-MCM-41, (c) Co/Al-MCM-41.

The appearance of these void defects amid the channels of the Co@Al-MCM-41 catalyst can also be supported by the pore size distributions (Fig. S3b), which presents a bimodal pore structure and is quite different from the unimodal pore distributions of the two other catalysts. The secondary pore is usually ascribed to the tensile strength effect and is actually another proof for the presence of the void defects.[4] Additionally, as expected, these voids were observed from the TEM (Fig. 1e) and STEM images (Fig.. 2d, e). We will come to this point later when discussing the FTS reaction results.

**ESI-6.** Fig. S4 Wide-angle XRD patterns of the samples.

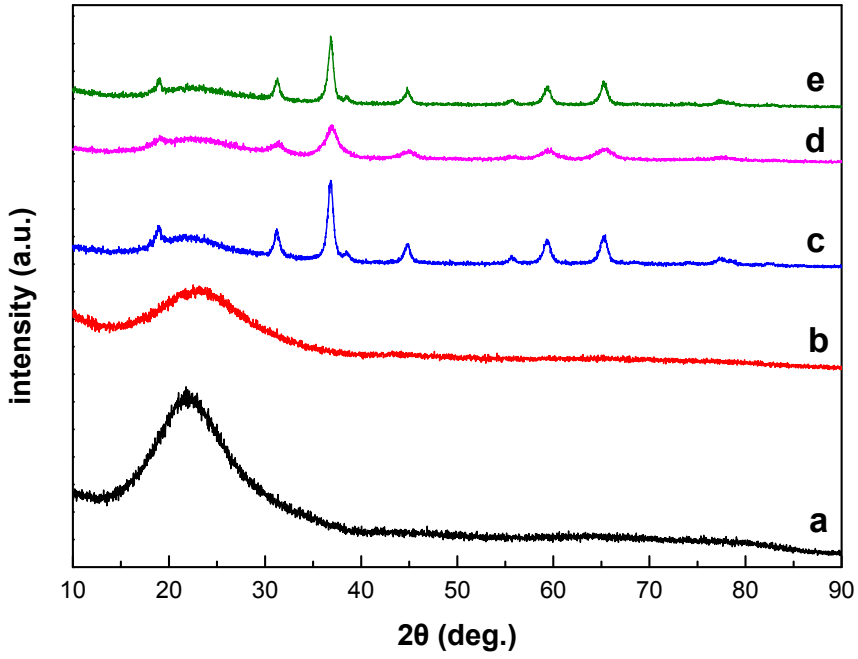


**Fig. S4.** Wide-angle XRD patterns of the samples: (a) $SiO_2$, (b) Al-MCM-41, (c) $Co/SiO_2$, (d) Co/Al-MCM-41, (e) Co@Al-MCM-41.

**ESI-7.**Table S2 $Co_3O_4$ particle size and elemental analysis of the catalysts.

**Table S2.** The properties of the obtained catalysts.

| Catalyst | $Co_3O_4$ particle size/nm | | Co content/% [c] | Si/Al ratio [c] | $Co^0$ particle size/nm [d] | $H_2$ uptake/μmol/g [d] |
|---|---|---|---|---|---|---|
| | I [a] | II [b] | | | | |
| $Co/SiO_2$ | 13.7 | 11.3 | 20.5 | — | 10.2 | 29.3 |
| Co@Al-MCM-41 | 13.2 | 10.6 | 21.0 | 46.8 | 10.4 | 28.2 |
| Co/Al-MCM-41 | 9.4 | 5.5 | 19.7 | 47.1 | 4.2 | 17.3 |

a Measured by the XRD pattern from the Scherrer formula .

b Evaluated from the particle size distributions of the discernible $Co_3O_4$ particles from several TEM images with high-resolution [5]

c Obtained from the XRF data.

d Determined by $H_2$ adsorption.

**ESI-8.** Fig. S5 Solid-state $^{27}$ Al MAS NMR spectra of the samples.

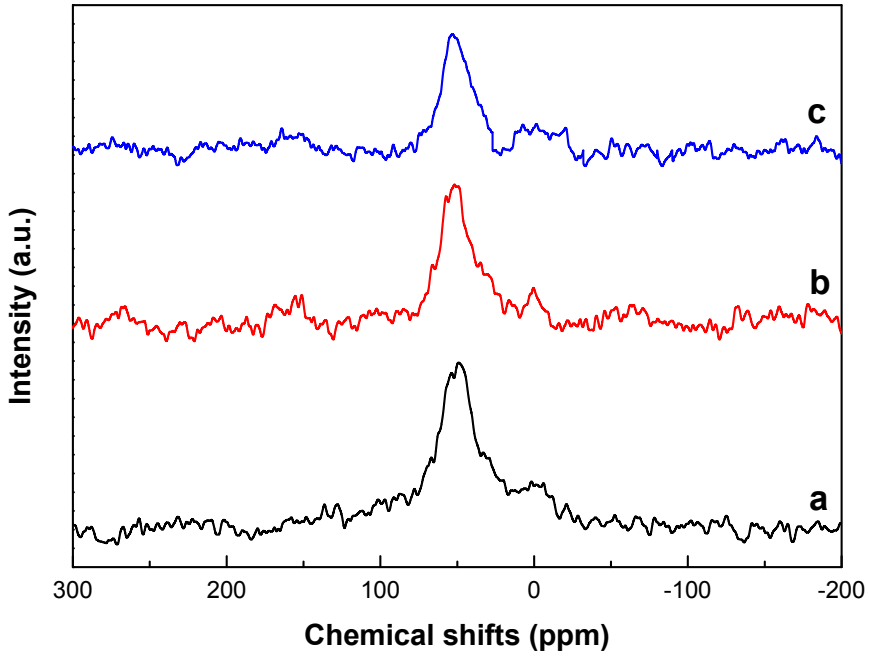


**Fig. S5.** Solid-state $^{27}$ Al MAS NMR spectra of the samples: (a) Al-MCM-41, (b) Co@Al-MCM-41, (c) Co/Al-MCM-41.

To investigate the quality, location and coordination state of aluminum in the samples, we conducted the solid-state characterization. As observed in Fig.7, the major peak centered at ca. 54 ppm can be assigned to the tetrahedrally coordinated framework aluminum ($AlO_4$), in which aluminum is covalently bound to four Si atoms via oxygen bridges.[6] The additional peak at ca. 0 ppm is assigned to the extra-framework aluminum with octahedral-coordinated chemical state.[7]

**ESI-9.** Fig. S6 $NH_3$-TPD patterns of the samples.

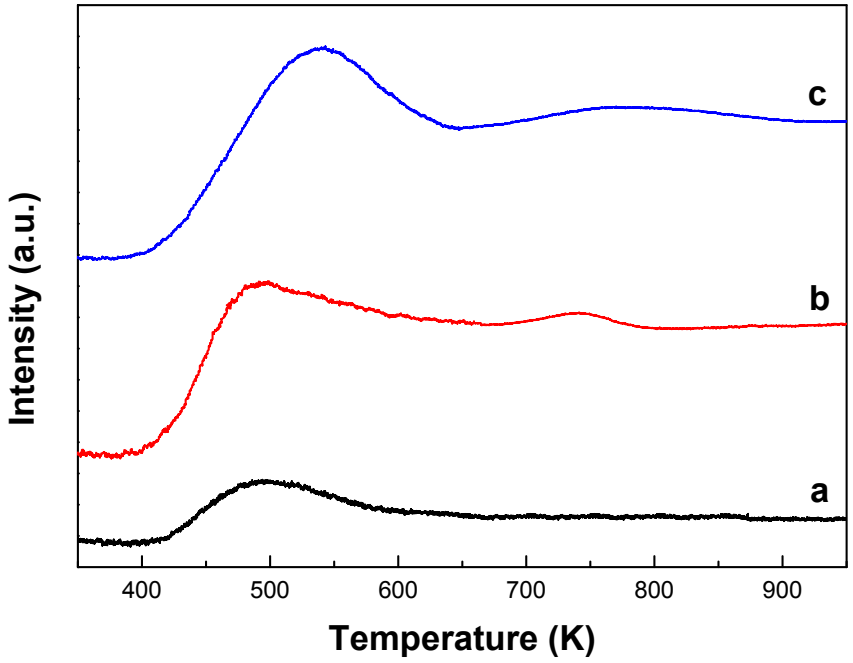


**Fig. S6.** $NH_3$-TPD patterns of the samples: (a) $Co/SiO_2$, (b) Co@Al-MCM-41, (c) Co/Al-MCM-41.

**ESI-10.** Fig. S7 $H_2$-TPR profiles of the samples.

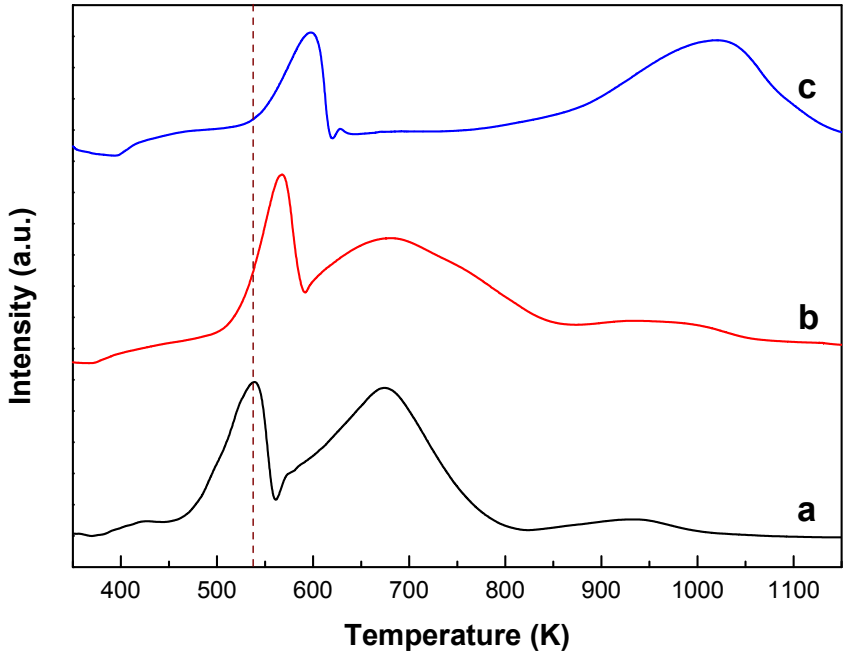


**Fig. S7.** $H_2$-TPR profiles of the samples: (a) $Co/SiO_2$, (b) Co@Al-MCM-41, (c) Co/Al-MCM-41.

The TPR profiles in the temperature range of 400-850 K of both $Co/SiO_2$ and Co@Al-MCM-41 catalysts, shown in Fig. S7, exhibit two peaks, corresponding to the two consecutive reduction steps of $Co_3O_4$ to metallic Co via the CoO intermediate.[8] The initiating temperature of Co@Al-MCM-41 is higher than that of $Co/SiO_2$ since the $Co_3O_4$ particles were compatibly imbedded into the uniform mesoporous silica. Besides these characteristics, a quite weak and broad peak located higher than 850 K was observed and can be assigned to the reduction of those cobalt oxides, which have a strong interaction with silica or aluminum components.[9] The TPR profile of the supported Co/Al-MCM-41 catalyst is much different from that of the above two samples, suggesting a different reduction behavior. The initiating temperature

was significantly retarded to 540 K, indicating a large diffusion barrier[10] for hydrogen molecules since the $Co_3O_4$ particles were rather small and highly dispersed or held in the one-dimensional channels, as confirmed by the above characterization and discussion. It has been reported that the dispersed small $Co_3O_4$ particles have a larger mutual interaction with the support than the large ones.[11] In addition, the second reduction peak is much weaker, while the third high-temperature peak becomes quite stronger,[12] compared with those of $Co/SiO_2$ and Co@Al-MCM-41. These observations demonstrate that the cobalt phase has a very intense mutual interaction with the Al-containing MCM-41 support, and thus a lot of inactive cobalt silicate and cobalt aluminate species can be generated, giving rise to the poor reducibility of this catalyst.

**ESI-11.** Fig. S8 XPS spectra of the catalysts.

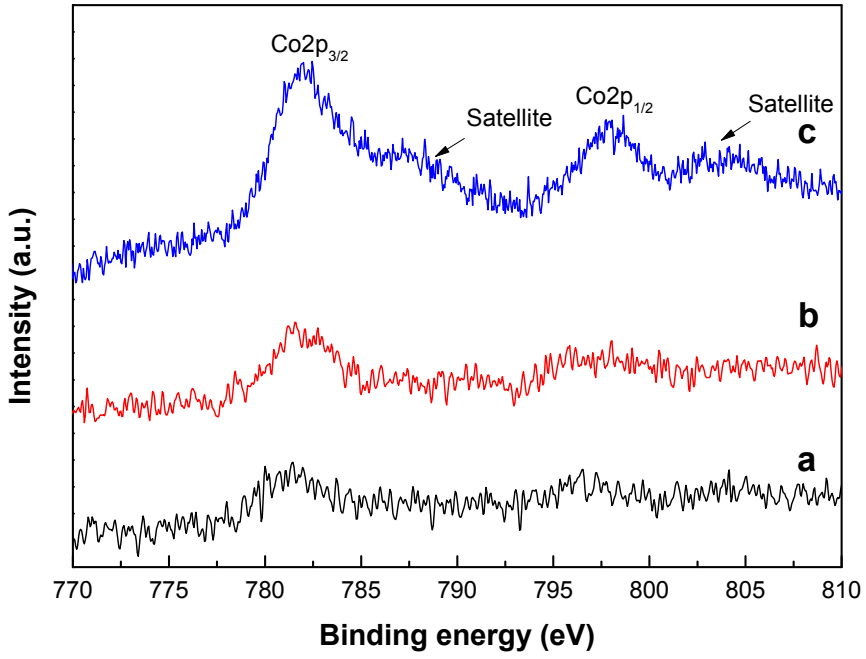


**Fig. S8.** XPS spectra of the catalysts: (a) $Co/SiO_2$, (b) Co@Al-MCM-41, (c) Co/Al-MCM-41.

For the impregnated Co/Al-MCM-41 catalyst, both $Co2p_{3/2}$ and $Co2p_{1/2}$ peaks shift towards the region of higher binding energies, meanwhile two high intensity of shake-up satellite peaks appeared and the spin-orbital splitting increases to 16.0 eV.[13] These features are indicative of the presence of hardly reducible $Co^{2+}$ species, probably in the form of cobalt silicate and cobalt aluminate, and strongly support our explanation that the cobalt species in the Co/Al-MCM-41 catalyst was intensively interacting with the Al-MCM-41 support.

**ESI-12.** Table S3 Reaction performance of the different catalysts.

**Table S3.** Reaction performance of the different catalysts [a]

| Catalyst | CO Conv./% | $CO_2$ Sel./% [b] | Sel./% | | | | | α [c] | $C_{iso}/C_n$ [d] | $C^{=}/C_n$ [e] |
|---|---|---|---|---|---|---|---|---|---|---|
| | | | $C_1$ | $C_2$-$C_4$ | $C_5$-$C_{12}$ | $C_{13}$-$C_{20}$ | $C_{20+}$ | | | |
| $Co/SiO_2$ | 83.1 | 6.49 | 13.5 | 16.3 | 49.8 | 18.2 | 2.31 | 0.87 | 0.08 | 0.07 |
| Co/Al-MCM-41 | 45.3 | 8.95 | 32.6 | 20.2 | 39.5 | 7.76 | 0 | 0.79 | 0.50 | 0.11 |
| Co@Al-MCM-41 | 78.1 | 5.97 | 14.3 | 9.89 | 64.5 | 10.7 | 0.55 | 0.83 | 1.36 | 0.18 |

a Reaction conditions: 1.0 MPa, 523 K, molar ratio of $H_2/CO$ = 2.0, W/F=5.0 gcat·h·$mol^{-1}$, time on stream 30 h.

b Analyzed by TCD.

c Chain growth probability.

d The molar ratio of *iso*-paraffins to *n*-paraffins in the range of $C_5$–$C_{12}$.

e The molar ratio of olefins to n-paraffins with $C_{2+}$.

**ESI-13.** Fig. S9 The SA-XRD patterns and WA-XRD patterns of the spent catalysts.

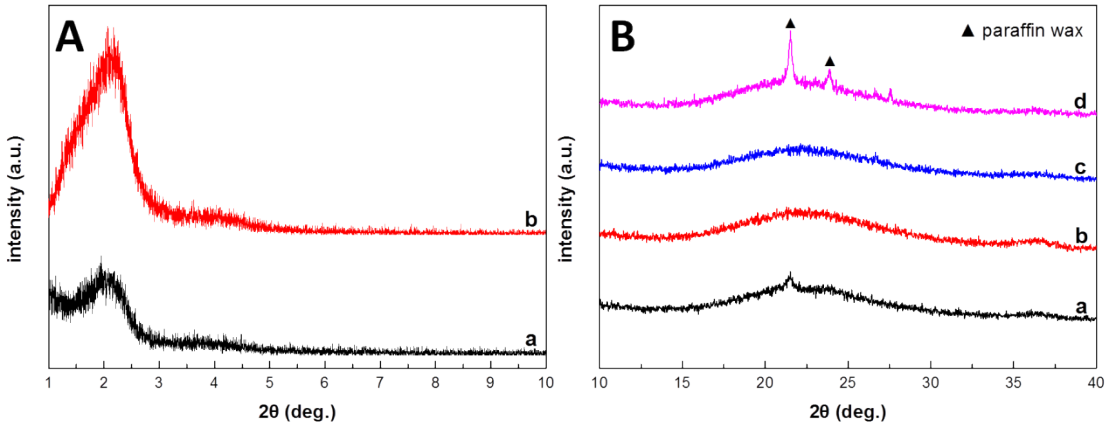


**Fig. S9.** (A) The SA-XRD patterns of the spent Co/Al-MCM-41 (a) and Co@Al-MCM-41 (b) catalysts. (B) The WA-XRD patterns of the spent catalysts: (a) $Co/SiO_2$, (b) Co/Al-MCM-41, (c) Co@Al-MCM-41 (FTS reaction at 523 K), (d) Co@Al-MCM-41 (FTS reaction at 503 K).

**ESI-14.** Detailed discussion on the methane selectivity in the Co/Al-MCM-41 catalyst.

There are several factors that can contribute to the high $CH_4$ selectivity in the Co/Al-MCM-41 catalyst. First of all, owing to the severe diffusion restriction, the actual $H_2$/CO ratio near the cobalt active sites can be very higher than the original ratio in the external gas phase due to the faster diffusion of $H_2$ molecules than CO.[14] Moreover, the effective $H_2$/CO ratio at the catalyst surface can be further increased on account of the presence of unreduced cobalt oxide species catalyzing the water-gas shift (WGS) reaction,[15] which can be strongly supported by the highest $CO_2$ selectivity obtained on the Co/Al-MCM-41 catalyst. It has been generally considered that the increase of local $H_2$/CO ratio near the surface $Co^0$ sites can promote the $CH_4$ formation.[15] What's more, small cobalt particle size would give rise to the yield of short-chain hydrocarbons,[16] and thus further enhancing the generation of $CH_4$. Furthermore, it is very likely that over-cracking of the hydrocarbons would take place due to the prolonged residence time and strong acidity of the Co/Al-MCM-41 catalyst.

## References


1. J. Y. Liu, J. F. Chen and Y. Zhang, *Catal. Sci. Technol.*, 2013, **3**, 2559–2564.

2. D. Schanke, S. Vada, E. A. Blekkan, A. M. Hilmen, A. Hoff and A.Holmen, *J. Catal.*, 1995, **156**, 85–95.

3. R. Mokaya, *Chem. Commun.*, 2001, **7**, 633–634.

4. Y. Li, Q. Yang, J. Yang and C. Li, *Microporous Mesoporous Mater.*, 2006, **91**, 85–91.

5. H. Li, J. Li, H. Ni and D. Song, *Catal. Lett.*, 2006, **110**, 71–76.

6. K. Chaudhari, T. K. Das, A. J. Chandwadkar and S. Sivasanker, *J. Catal.*, 1999, **186**, 81–90.

7. M. Xu, W. Wang, M. Seiler, A. Buchholz and M. Hunger, *J. Phys. Chem. B*, 2002, **106**, 3202–3208.

8. W. D. Shafer, G. Jacobs and B. H. Davis, *ACS Catal.*, 2012, **2**, 1452–1456.

9. J. Panpranot, J. G. Goodwin Jr and A. Sayari, *Catal. Today*, 2002, **77**, 269–284.

10. R. Guettel, J. Knochen, U. Kunz, M. Kassing and T. Turek, *Ind. Eng. Chem. Res.*, 2008, **47**, 6589–6597.

11. A. Y. Khodakov, A. Griboval-Constant, R. Bechara and V. L. Zholobenko, *J. Catal.*, 2002, **206**, 230–241.

12. S. Lim, D. Ciuparu, Y. Chen, L. Pfefferle and G. L. Haller, *J. Phys. Chem. B*, 2004, **108**, 20095–20101.

13. S. G. Aspromonte, Á. Sastre, A. V. Boix, M. J. Cocero and E. Alonso, *Microporous Mesoporous Mater.*, 2012, **148**, 53–61.

14. D. Vervloet, F. Kapteijn, J. Nijenhuis and J. R. van Ommen, *Catal. Sci. Technol.*, 2012, **2**, 1221–1233.

15. A. Martínez, C.López, F. Márquez and I. Díaz, *J. Catal.*, 2003, **220**, 486–499.

16. G. L. Bezemer, J. H. Bitter, H. P. C. E. Kuipers, H. Oosterbeek, J. E. Holewijn, X. Xu, F. Kapteijn, A. J. van Dillen and K. P. de Jong, *J. Am. Chem. Soc.*, 2006, **128**, 3956–3964.